JOC Article

Experimental and Computational Studies of Ring Inversion of 1,4-Benzodiazepin-2-ones: Implications for Memory of Chirality Transformations

Polo C.-H. Lam and Paul R. Carlier*

Department of Chemistry, Virginia Tech, Blacksburg, Virginia 24061

pcarlier@vt.edu

Received September 2, 2004

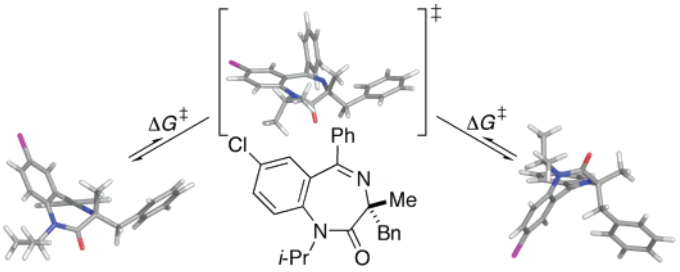

We recently reported the enantioselective syntheses of quaternary 1,4-benzodiazepin-2-ones via memory of chirality. The success of this method depends on formation of conformationally chiral enolates that racemize very slowly under the reaction conditions. As a prelude to undertaking experimental and computational studies on the racemization of these enolates, we have studied the ring-inversion process of the parent 1,4-benzodiazepin-2-ones. In this paper, we use dynamic and 2D-EXSY NMR to characterize inversion barriers. Using DFT calculations, we reproduce the experimental results with high accuracy (within 1−2 kcal/mol). Structural parameters obtained from DFT calculations provide valuable insights into the important effect of the N1 substituent on the ring-inversion barrier and shed light on the mechanism of the memory of chirality method. These measurements and calculations provide a foundation for future studies of benzodiazepine enolates and will be valuable in the design of new memory of chirality reactions.

Introduction

1,4-Benzodiazepines are among the most important scaffolds in medicinal chemistry.[1−3] Representative members of this class have shown activity as anxiolytics[4,5] and as antagonists of CCK-A,[6,7] $GABA_A$ receptor,[8] human bradykinin B2,[9] and HIV-1 Tat receptors.[10] These drugs have also proven useful as inhibitors of Ras farnesylation[11] and Src protein tyrosine kinase[12] and have shown anti-arrhythmic activity.[13] Therefore experimental and computational studies of the conformational dynamics of these drugs have intrinsic value. Furthermore, 1,4-benzodiazepine anxiolytics are known to exert their effect by inducing a conformational change at the GABA(A) receptor.[14] The possibility that ring inversion of these drugs plays some role in the induced conformational change of the receptor provides additional impetus for our studies.

Most of the 1,4-benzodiazepines investigated to date have been prepared from proteinogenic amino acid derivatives or their enantiomers, and thus carry the α-proton from its parent amino acid. Structurally related enantiopure 3,3-disubstituted "quaternary" benzodiaz-

(1) Evans, B. E.; Rittle, K. E.; Bock, M. G.; DiPardo, R. M.; Freidinger, R. M.; Whitter, W. L.; Lundell, G. F.; Veber, D. F.; Anderson, P. S.; Chang, R. S. L.; Lotti, V. J.; Cerino, D. J.; Chen, T. B.; Kling, P. J.; Kunkel, K. A.; Springer, J. P.; Hirschfield, J. *J. Med. Chem.* **1988**, *31*, 2235−2246.

(2) Ellman, J. A. *Acc. Chem. Res.* **1996**, *29*, 132−143.

(3) Sternbach, L. H. *J. Med. Chem.* **1979**, *22*, 1−7.

(4) Maksay, G.; Tegyey, Z.; Simonyi, M. *Mol. Pharmacol.* **1991**, *39*, 725−732.

(5) Molewijk, H. E.; Hartog, K.; Vanderpoel, A. M.; Mos, J.; Olivier, B. *Psychopharm.* **1996**, *128*, 31−38.

(6) Evans, B. E.; E., R. K.; Bock, M. G.; DiPardo, R. M.; Freidinger, R. M.; Whitter, W. L.; Gould, N. P.; Lundell, G. F.; Homnick, C. F.; Veber, D. F.; Anderson, P. S.; Chang, R. S. L.; Lotti, V. J.; Cerino, D. J.; Chen, T. B.; King, P. J.; A., K. K.; Springer, J. P.; Hirschfield, J. *J. Med. Chem.* **1987**, *30*, 1229−1239.

(7) Willson, T. M.; Henke, B. R.; Momtahen, T. M.; Meyers, P. L.; Sugg, E. E.; Unwalla, R. J.; Croom, D. K.; Dougherty, R. W.; Grizzle, M. K.; Johnson, M. F.; Queen, K. L.; Rimele, T. J.; Yingling, J. D.; James, M. K. *J. Med. Chem.* **1996**, *39*, 3030−3034.

(8) Li, X.; Cao, H.; Zhang, C.; Furtmueller, R.; Fuchs, K.; Huck, S.; Sieghart, W.; Deschamps, J.; Cook, J. M. *J. Med. Chem.* **2003**, *46*, 5567−5570.

(9) Dziadulewicz, E. K.; Brown, M. C.; Dunstan, A. R.; Lee, W.; Said, N. B.; Garratt, P. J. *Bioorg. Med. Chem. Lett.* **1999**, *9*, 463−468.

(10) Hsu, M.-C.; Schutt, A. D.; Holly, M.; Slice, L. W.; Sherman, M. I.; Richman, D. D.; Potash, M. J.; Volsky, D. J. *Science (Washington, D.C.)* **1991**, *254*, 1799−1802.

10.1021/jo048450n CCC: $30.25
Published on Web 02/05/2005

SCHEME 1. General Reaction Scheme for the Enantioselective Alkylation of BZDs[22]

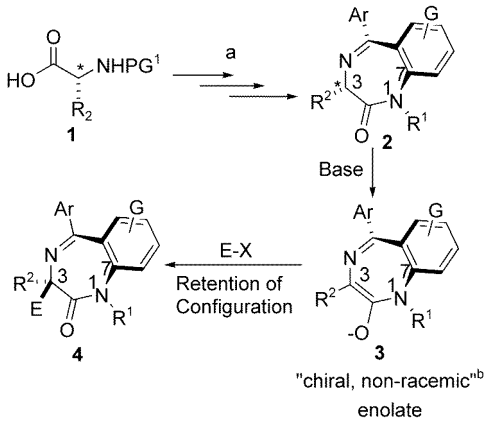

[a] Standard protocol.[22,30] [b]Although structure **3** contains no permanent chiral center, it is transiently chiral due to the nonplanar ring.

epines have rarely been explored,[15−18] despite their potential usefulness, due to the fact that the corresponding quaternary amino acids[19] are generally not commercially available.[20,21] To enable the enantioselective syntheses of "quaternary" benzodiazepines, we have recently reported an enantioselective α-alkylation route[22] that relies upon a "memory of chirality" mechanism.[23−29] Our approach is shown in Scheme 1: the parent 1,4-benzodiazepin-2-one (henceforth BZD) **2** is synthesized from the corresponding proteinogenic amino acid **1** using a modification of Shea's protocol.[30] Deprotonation by base at low temperature generates a chiral, nonracemic enolate **3**, which is alkylated by electrophile with retention of configuration to generate the 3,3-disubstituted BZDs **4** with high (up to 99%) ee.[22]

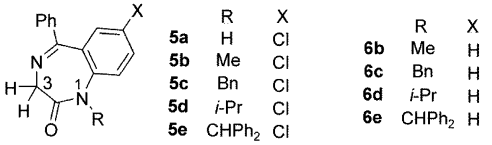

	R	X
5a	H	Cl
5b	Me	Cl
5c	Bn	Cl
5d	*i*-Pr	Cl
5e	$CHPh_2$	Cl

	R	X
6b	Me	H
6c	Bn	H
6d	*i*-Pr	H
6e	$CHPh_2$	H

FIGURE 1. Coalescence temperature study of compound **5a**−**e** and computational study of their des-chloro analogues **6b**−**e**.

The success of this reaction is dependent upon the following factors: (1) the conformational chirality of the BZD ring that "memorized" the chirality of the stereogenic center at C3; (2) The formation of enolate **3** with retention of chiral information in the ring conformation; (3) the slow racemization of **3** via ring inversion under the reaction conditions; and (4) the stereoselective electrophilic trapping of **3** to form enantiomerically enriched "quaternary" BZD **4**.

In this paper, we will present physical and computational studies of the conformational chirality of the BZD ring exemplified by **2**. These studies will lay a foundation for future studies of BZD enolates and provide insights into the "memory of chirality" mechanism we have proposed.

Results and Discussion

Coalescence Temperature Measurements of Glycine-Derived BZD 5b−e. Despite the absence of a stereogenic center, glycine-derived BZDs such as **5a**−**e** are chiral, as a consequence of the nonplanar ring conformation (Figure 1).[31,32] At room temperature, the C3 protons of **5b**−**e** exist as two discrete doublets in the ^{1}H NMR spectra. For **5a**, the two C3 protons appear as a broad singlet, indicating a fast ring inversion on the ^{1}H NMR time scale. The inversion barrier $\Delta G_c^{\ddagger}$ for **5a**−**d** in deuteriopyridine and hexachlorobutadiene has already been determined by Lehn[31] using coalescence temperature measurements with 60 MHz NMR and the standard equations.[33−35]

In the studies conducted by Lehn[31] and by Gilman,[36] both authors noted that the inversion barrier of BZDs depends on the size of the N1 substituent. We also observed that the inversion barrier of BZDs increases with increasing size of the N1 substituent in our preliminary study of **5b** and **5d**.[22] However, Lehn's reported

(11) James, G. L.; Goldstein, J. L.; Brown, M. S.; Rawson, T. E.; Somers, T. C.; McDowell, R. S.; Crowley, C. W.; Lucas, B. K.; Levinson, A. D.; Masters, J. C. *Science (Washington, D.C.)* **1993**, *260*, 1937−1942.
(12) Ramdas, L.; Bunnin, B. A.; Plunkett, M. J.; Sun, G.; Ellman, J.; Gallick, G.; Budde, R. J. A. *Arch. Biochem. Biophys.* **1999**, *368*, 394−400.
(13) Selnick, H. G.; Liverton, N. J.; Baldwin, J. J.; Butcher, J. W.; Claremon, D. A.; Elliott, J. M.; Freidinger, R. M.; King, S. A.; Libby, B. E.; McIntyre, C. J.; Pribush, D. A.; Remy, D. C.; Smith, G. R.; Tebben, A. J.; Juriewicz, N. K.; Lynch, J. J.; Salata, J. J.; Sanguinetti, M. C.; Siegl, P. K. S.; Slaughter, D. E.; Vyas, K. *J. Med. Chem.* **1997**, *40*, 3865−3868.
(14) Williams, D. B.; Akabas, M. H. *Mol. Pharmacol.* **2000**, *58*, 1129−1136.
(15) Confalone, P. N.; Huie, E. M.; Ko, S. S.; Cole, G. M. *J. Org. Chem.* **1988**, *53*, 482−487.
(16) Wright, W. B., Jr.; Brabander, H. J.; Greenblatt, E. N.; Day, I. P.; Hardy, R. A., Jr. *J. Med. Chem.* **1978**, *21*, 1087−1089.
(17) Reitter, B. E.; Sachdeva, Y. P.; Wolfe, J. F. *J. Org. Chem.* **1981**, *46*, 3945−3949.
(18) Simonyi, M.; Kaksay, G.; Kovacs, I.; Tegyey, Z.; Parkanyi, L.; Kalman, A.; Otvos, L. *Bioorg. Chem.* **1990**, *18*, 1−12.
(19) Cativiela, C.; Díaz-de-Vellagas, M. D. *Tetrahedron: Asymmetry* **1998**, *9*, 3517−3599.
(20) Avdagic, A.; Lesac, A.; Majer, Z.; Hollosi, M.; Sunjic, V. *Helv. Chim. Acta* **1998**, *81*, 1567−1582.
(21) Avdagic, A.; Sunjic, V. *Croat. Chem. Acta* **2000**, *73*, 743−753.
(22) Carlier, P. R.; Zhao, H.; DeGuzman, J.; Lam, P. C.-H. *J. Am. Chem. Soc.* **2003**, *125*, 11482−11483.
(23) Seebach, D.; Wasmuth, D. *Angew. Chem., Int. Ed. Engl.* **1981**, *20*, 971.
(24) Seebach, D.; Sting, A. R.; Hoffman, M. *Angew. Chem., Int. Ed. Engl.* **1996**, *35*, 2708−2748.
(25) Kawabata, T.; Yahiro, K.; Fuji, K. *J. Am. Chem. Soc.* **1991**, *113*, 9694−9696.
(26) Fuji, K.; Kawabata, T. *Chem. Eur. J.* **1998**, *4*, 373−376.
(27) Kawabata, T.; Suzuki, H.; Nagae, Y.; Fuji, K. *Angew. Chem., Int. Ed.* **2000**, *39*, 2155−2157.
(28) Wanyoike, G. N.; Onomura, O.; Maki, T.; Matsumura, Y. *Org. Lett.* **2002**, *4*, 1875−1877.
(29) Brewster, A. G.; Jayatissa, J.; Mitchell, M. B.; Schofield, A.; Stoodley, R. J. *Tetrahedron Lett.* **2002**, *43*, 3919−3922.
(30) Hart, B. R.; Rush, D. J.; Shea, K. J. *J. Am. Chem. Soc.* **2000**, *122*, 460−465.
(31) Linscheid, P.; Lehn, J.-M. *Bull. Chim. Soc. Fr.* **1967**, 992−997.
(32) Konowal, A.; Snatzke, G.; Alebic-Kolbah, T.; Kajfez, F.; Rendic, S.; Sunjic, V. *Biochem. Pharm.* **1979**, *28*, 3109−3113.
(33) $\Delta G_c^{\ddagger} = 4.58\ T_c(10.32 + \log T_c/k_c)$ cal mol^{-1} (1), $k_c = 2.22\ (\Delta\nu^2 + 6J_{AB}^2)^{1/2}$ (2). Here, T_c is the coalescence temperature, k_c is the exchange rate constant at coalescence temperature, $\Delta\nu$ is the separation of the two coalescing proton signals in Hz at room temperature, and J_{AB} is the coupling constant of the two proton signals with each other.
(34) Bain, A. D. *Prog. Nucl. Magn. Reson. Spectrosc.* **2003**, *43*, 63−103.
(35) Friebolin, H. *Basic one- and two-dimensional NMR spectroscopy*; 3rd rev. ed.; Wiley-VCH: Weinheim, 1998; pp xxiv, 386.
(36) Gilman, N. W.; Rosen, P.; Earley, J. V.; Cook, C.; Todaro, L. J. *J. Am. Chem. Soc.* **1990**, *112*, 3969−3978.

TABLE 1. Coalescence Temperature Measurements of 5b−e and Their Corresponding Inversion Barriers[a]

compd	signal	$\Delta\nu^b$ (Hz)	$J_{AB}{}^c$ (Hz)	$T_c{}^d$ (K)	$\Delta G_c^{\ddagger\,e}$ (kcal/mol)	lit. value[31,f] (kcal/mol)
5b	C3−CH_2	316	10.8	391	18.0 ± 0.2	17.8, 17.6[g]
5c	C3−CH_2	301	10.6	422	19.5 ± 0.2	19.3
	Bn-CH_2	232	15.8	416	19.5 ± 0.2	19.2
5d	C3−CH_2	306	10.6	>458[h]	>21.3[i]	19.2[j]
	i-Pr−CH_3	89.4	0[k]	437	21.3 ± 0.2	18.7
5e	C3−CH_2	238	10.8	458	21.5 ± 0.2	N/A

[a] The C3 protons of **5a** appear as a broad singlet at room temperature, and we did not explore low-temperature decoalescence of **5a**. [b] The separation between the two coalescing proton signals at room temperature in Hz. [c] The coupling constant between the two coalescing proton signals at room temperature. [d] Coalescence temperature. [e] Inversion barrier, calculated from the coalescence temperature measurements and eqs 1 and 2; the stated error reflects an uncertainty in T_c of ± 3 K. [f] Lehn measured the coalescence temperature for **5b**−**d** with 60 MHz NMR. [g] These two numbers are both taken from Lehn's original paper. [h] The C3 protons fail to coalesce at 458 K, the highest attainable temperature of our 400 MHz NMR module. [i] The lower bound value calculated using 458 K as coalescence temperature; the estimated upper bound value is 21.7 kcal/mol, see text. [j] In our experiments, **5d** clearly has a higher inversion barrier than **5c**, an observation that differs from Lehn's report. [k] The protons of the diastereotopic Me groups do not couple each other.

inversion barrier for **5d** (18.7−19.2 kcal/mol) was significantly smaller than our measured value (21.3-21.7 kcal/mol); furthermore, their value is smaller than that of **5c** and seems to depart from the overall trend of the series. Therefore, we present here the details of our coalescence temperature (T_c) measurement of **5b** and 5**d**, with new data on **5c** and **5e**, all of which were performed in DMSO-d_6 at 400 MHz (Table 1). We estimate our uncertainty in T_c as ±3 K.

For **5b**, the coalescence temperature for the C3 CH_2 is 391 K, corresponding to an inversion barrier of 18.0 ± 0.2 kcal/mol. For **5c**, two sets of protons, C3 CH_2 and Bn CH_2, are brought to coalesce at 422 and 416 K, respectively. Both of these coalescences indicate the same barrier of 19.5 kcal/mol. For **5d**, the coalescence temperature of the *i*-Pr Me group was found to be 437 K, which gives an inversion barrier of 21.3 kcal/mol. This number, however, should only be taken as a lower bound because the C3 CH_2 did not coalesce at our highest possible operating temperature (458 K), indicating an inversion barrier of greater than 21.3 kcal/mol. Qualitative comparison with spectra of **5b**,**c**,**e** suggested that the coalescence temperature of **5d** is within 5−10° of 458 K (i.e., 463−468 K), which gives an upper bound of 21.7 kcal/mol. For **5e**, the C3 CH_2 coalesced at 458 K, corresponding to an inversion barrier of 21.5 kcal/mol. It should be noted that although the measured inversion barrier for **5d** is slightly lower than that of **5e**, we are comparing two different sets of protons in the process. The fact that the C3 CH_2 of **5d** fails to coalesce at 458 K shows that **5d** should have inversion barrier of 21.3-21.7 kcal/mol, comparable to that of **5e**.

The results for **5b**, reported earlier in our communication,[22] and **5c** are in close agreement with Lehn's results. Our measured value for **5d** is definitely higher than that of Lehn's. In their study, the C3 CH_2 of **5d** coalesced at a temperature lower than that of **5c**, a result that is difficult to reconcile. Our study in contrast shows a steady increase in the barrier as the steric bulk of the N1 substituent is increased from Me to Bn to *i*-Pr.

DFT Calculations of Ring-Inversion Barriers of Glycine-Derived BZDs. To better understand the ring-inversion process of **5b**−**e**, we performed density functional theory (DFT) calculations.[37,38] An excellent earlier

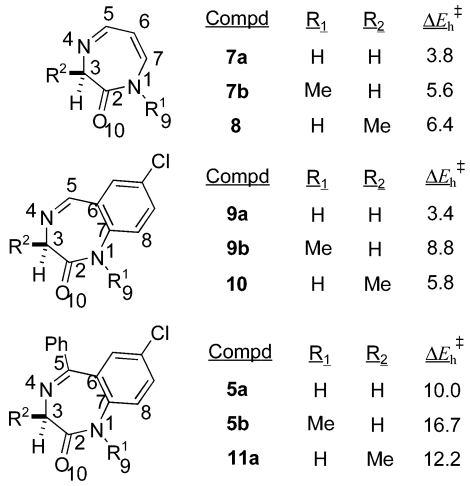

FIGURE 2. Summary of Paizs's calculations of benzodiazepine ring inversion barrier at the B3LYP/6-31G(d) level.[39] The ring inversion barriers $\Delta E_h^{\ddagger}$ were calculated from the zero-point vibrational energy corrected electronic energy E_h, in kcal/mol.

DFT computational study of BZDs was reported by Paizs.[39] These authors focused mainly on the effect of the annulated benzo and C5 Ph ring on the geometry of the ring inversion transition structure and did not comprehensively explore the effect of the N1 substituent on the ring-inversion barrier. Structures studied by Paizs, and the computed ring-inversion barriers, are shown in Figure 2. Paizs noted that the B3LYP/6-31G(d) level reproduced Lehn's reported barrier of **5b** to within 1 kcal/mol.

In our work, the equilibrium and ring-inversion transition geometry were optimized at B3LYP/6-31G(d). Vibrational frequencies were calculated at the same level to determine the zero-point vibrational energies (ZPVE) and the thermal corrections to the Gibbs free energies. The calculated ring-inversion transition structures were verified by their single imaginary frequency, the displacement vectors of which corresponded to the distortion from the "flat" transition structure toward the equilibrium geometry. The ring-inversion barrier is thus calculated by the corrected energy difference between the transition structure and the equilibrium geometry. To reduce calculation time, we substituted the des-chloro BZDs **6c**−**e** for **5c**−**e** in our calculations. The results are summarized in Table 2.

(37) Jalbout, A. F.; Nazari, F.; Turker, L. *THEOCHEM* **2004**, *671*, 1−21.
(38) Geerlings, P.; De Proft, F.; Langenaeker, W. *Chem. Rev.* **2003**, *103*, 1793−1873.
(39) Paizs, B.; Simonyi, M. *Chirality* **1999**, *11*, 651−658.

TABLE 2. B3LYP/6-31+G(d)//B3LYP/6-31G(d)-Calculated Inversion Barriers (kcal/mol) for BZDs 5b and Des-chloro BZDs 6b−e[a]

		B3LYP/6-31G(d)	B3LYP/6-31+G(d)//B3LYP/6-31G(d)				
compd	N1 subs	$\Delta E_h^{\ddagger}$[b]	$\Delta E_h^{\ddagger}$[c]	$\Delta G^{\ddagger}$ (298 K)[d]	$\Delta G^{\ddagger}$ (T_c)[e]	$\Delta G^{\ddagger}$ (T_c, DMSO)[f]	exptl inversion barrier for **5b−e**[g]
5b	Me	17.3	17.6	17.0	17.0	16.8	18.0 ± 0.2 (391 K)
6b	Me	17.4	17.7	16.9	16.8	16.9	18.0 ± 0.2 (391 K)
6c	Bn	17.8	17.6	18.0	18.3	17.8	19.5 ± 0.2 (422 K)
6d	*i*-Pr	20.2	20.2	20.7	21.2	21.6	21.3−21.7 (>458 K)[h]
6e	$CHPh_2$	18.9	19.2	19.5	19.8	20.8	21.5 ± 0.2 (458 K)
RMSD[i]		1.5	1.4	1.3	1.2	1.1	

[a] All structures are optimized at the B3LYP/6-31G(d) level. For economy, the des-chloro BZD analogues **6c**,**d** were studied. The effect of the Cl atom on the calculated inversion barriers is minimal, as seen from the first two rows. [b] Calculated from electronic energies at B3LYP/6, corrected by ZPVE. [c] Calculated from electronic energies at B3LYP/6-31+G(d)//B3LYP/6-31G(d), corrected by ZPVE. [d] Calculated from the B3LYP/6-31+G(d) single point energy, including the Gibbs free energy correction calculated at B3LYP/6-31G(d) level at 298 K. [e] Calculated from the B3LYP/6-31+G(d) single point energy, including the Gibbs free energy correction calculated at B3LYP/6-31G(d) level at the corresponding coalescence temperature T_c. [f] Calculated from B3LYP/6-31+G(d) single-point energy in DMSO using Tomasi's polarized continuum model (PCM), including the Gibbs free energy correction at T_c. [g] The stated errors in the inversion barrier are based on an estimated error in T_c of ±3 K. For des-chloro BZDs **6b−e**, the inversion barriers for their corresponding BZDs **5b−e** are used. Numbers in parentheses are the coalescence temperatures. [h] Based on the C3-CH_2 of **5d**, the coalescence temperature is above 458 K, which gives a lower bound value for the inversion barrier of 21.3 kcal/mol and an upper bound value of 21.7 kcal/mol. [i] The root-mean-square derivations of the calculated value from the experimental value for that method. The lower bound value of 21.3 kcal/mol for **5d** was used.

Our $\Delta E_h^{\ddagger}$ at B3LYP/6-31G(d) for **5b** is within 1 kcal/mol of that obtained by Paizs, who incorporated the ZPVE correction at 6-31G rather than 6-31G(d). Comparison of the inversion barrier of **5b** and **6b** (its des-chloro analogue) shows minimal effect of the chlorine atom on the resultant inversion barrier and thus our omission of the chlorine atom appears justified. To compare our calculations for **6b−e** with the experimentally determined values for the chloro analogues **5b−d** we calculated the single point energies at B3LYP/6-31+G(d) and applied the Gibb's free energy correction at B3LYP/6-31G(d). The effect of DMSO solvation was estimated using Tomasi's PCM model.[40,41] In this way the deviation of the calculated barriers for **6b−e** from the experimental barrier for **5b−e** decreases from an RMSD of 1.5 kcal/mol for $\Delta E_h^{\ddagger}$ to an RMSD value of 1.1 for $\Delta G^{\ddagger}$ (T_c, DMSO). Given the small range of inversion barrier (3.5 kcal/mol) from **5b** to **5e**, density functional theory performs reasonably well, reproducing both the rank order and the inversion barriers themselves. In contrast, we found that use of MP2/6-31G-(d) single-point energies significantly overestimates the inversion barrier (RMSD 2.7 kcal/mol, data not shown).

Calculated Structural Features of Glycine-Derived BZD Equilibrium Geometries and Ring-Inversion Transition Structures. In addition to studying the effect of the N1 substituent size on the inversion barrier, we also studied its effect on the equilibrium and ring-inversion transition structure geometries; DFT is known to generate structural parameters comparable with a higher level of calculations.[42] Our initial assumption was that increasing the size of the N1 substituent would simply increase the unfavorable van der Waals contact in the ring-inversion transition structures. However, as will be shown below, increasing size of the N1 substituent also appears to increase the inversion barrier by partially disrupting amide resonance in the ring-inversion transition structures (vide infra).

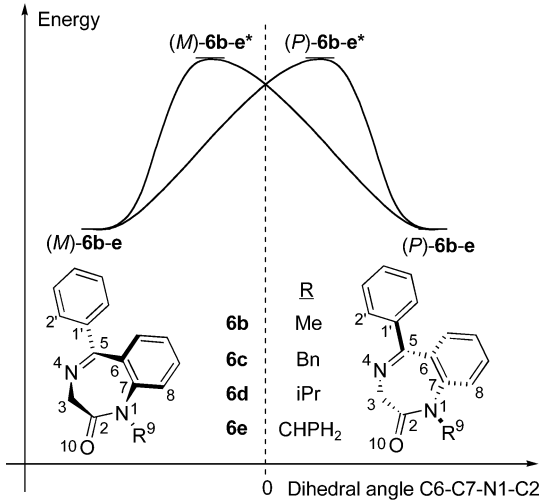

FIGURE 3. Calculated ring inversion energy profile for BZDs **6b−e**. There are two ring-inversion transition structures, (*M*)-**6*** and its enantiomer (*P*)-**6***, due to the fact that the **6*** is not of C_s symmetry. Note that the sign of the dihedral angle C6−C7−N1−C2 defines the helical chirality descriptor (*M* or *P*); the sign of this dihedral angle also matches that of C8−C7−N1−C9 (Table 3).

The most important feature of the ring-inversion process according to our calculation is that, in the ring inversion transition structure **5b*** and **6b*−e***, the seven-membered BZD ring is nearly, but not perfectly flat. This distortion from C_s symmetry was seen by Paizs for **5b***[39] and indicates that in going from the (*M*)-conformer to the (*P*)-conformer, there are two equienergetic pathways which pass through either one of the two enantiomeric transition structures (Figure 3). To confirm that these two enantiomeric transition structures indeed connect the enantiomeric equilibrium geometries, IRC calculations were performed using (*M*)- and (*P*)-**6d*** as starting geometries. In each case IRC calculations found the equilibrium geometries (*M*) and (*P*)-**6d** on opposite sides of the potential.

Most of the dihedral angles of the BZD equilibrium geometries show little change with increasing size of the N1 substituent, except for the angles C8−C7−N1−C9

(40) Tomasi, J.; Cammi, R.; Mennucci, B.; Cappelli, C.; Corni, S. *Phys. Chem. Chem. Phys.* **2002**, *4*, 5697−5712.
(41) Luque, F. J.; Curutchet, C.; Muñoz-Muriedas, J.; Bidon-Chanal, A.; Soteras, I.; Morreale, A.; Gelpi, J. L.; Orozco, M. *Phys. Chem. Chem. Phys.* **2003**, *5*, 3827−3836.

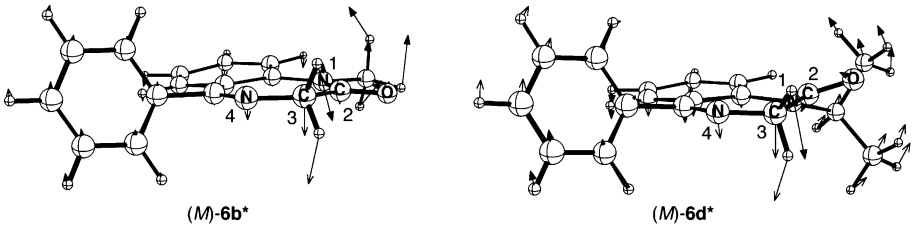

FIGURE 4. Effect of N1 substituent size on the ring-inversion transition structure: The C2 carbonyl group and N1 *i*-Pr group on **6d*** are twisted out of plane to avoid steric crowding, in contrast to the more planar **6b*** featuring the smaller N1 Me group. The arrows correspond to the vector of the single imaginary vibrational frequency, which distort the transition structure back to the equilibrium geometry.

TABLE 3. Selected Structural Parameters for Glycine-Derived BZDs Equilibrium Geometries[a]

	equilibrium geometry			ring inversion transition structure (*M*)-**5b***, **6b***−**6e***		
compd	∠C8−C7−N1−C9 (deg)	∠C9−N1−C2−O10 (deg)	sum of internal ∠[b] (deg)	∠C8−C7−N1−C9 (deg)	∠C9−N1−C2−O10 (deg)	sum of internal ∠[b] (deg)
(*M*)-**5b**	−33.9	−2.4	835.2	−5.9	0.3	899.2
(*M*)-**6b**	−33.8	−2.3	835.2	−7.0	2.0	899.5
(*M*)-**6c**	−44.2	3.9[c]	834.3	−14.2	10.1	898.9
(*M*)-**6d**	−43.3	2.1[c]	832.6	−18.9	23.1	889.0
(*M*)-**6e**	−51.1	7.1[c]	831.7	−22.4	28.3	887.9

[a] All angles are measured on the (*M*)-conformer, defined by the N1−C7 axis. [b] Sum of the seven internal bond angles in the BZD's seven-membered ring. [c] A change of sign in this dihedral angle does not affect the (*M*)- and (*P*)-conformer assignment, as this is defined by the sign of ∠C8−C7−N1−C9.

and C9−N1−C2−O10, which increase as consequence of the proximity of the N1 substituent and its neighboring C8 and C2 carbonyl, respectively (Table 3).

When the N1 substituent size increases from Me (**5b** and **6b)** to $CHPh_2$ (**6e)**, ∠C8−C7−N1−C9 increases by 17°. A smaller increase in ∠C9−N1−C2−O10 is seen in the series from **5b/6b** to **6e**, likely because amide resonance constrains ∠C9−N1−C2−O10 to remain close to 0°. In all of these structures N1 remains planar (sum of angles at N1 = 359−360°).

For the ring-inversion transition structures **5b*** and **6b***−**e***, a planar N1 is also seen (sum of angles = 360°), and ∠C8−C7−N1−C9 is smaller than that in the corresponding equilibrium geometries, because ring inversion requires C9 (the R group at N1) to approach an eclipsing orientation with its neighboring C8. However, for the larger R groups (**6d*** and **6e*)** this dihedral angle is significantly non-zero, apparently because the larger R group precludes eclipsing of C8 and C9. Similarly for smaller R groups, ∠C9−N1−C2−O10 is close to 0°, consistent with a near-planar ring-inversion transition structure. In contrast, for larger R groups (**6d*** and **6e*)**, this angle is significantly non-zero and larger than it is in equilibrium geometries **6d** and **6e**, indicating disruption of amide resonance (Figure 4). This loss of amide resonance may be a consequence of stronger steric interaction between extraannular substituents in the transition structures than in the equilibrium geometries.

The increased steric interaction between extraannular substituents in the ring inversion transition structures (in particular the C2 carbonyl O and N1 R) is a natural geometric consequence of the flattening of the BZD ring. In the equilibrium geometries **5b**, **6b**−**e** the sum of the internal angles ranges from 831 to 835°, consistent with the value of 829° calculated from simple VSEPR considerations.[43] However, in the ring inversion transition structures **5b***, **6b***−**e*** the sum of the internal angles ranges from 888 to 900°, consistent with the calculated 900° for a heptagon.[44] As the internal angles increase, the external angles of the nearly flat ring atoms necessarily decrease, forcing the extraannular substituents closer together.

DFT Calculations of C3 Monosubstituted BZD 12d. For the glycine-derived BZDs **5** and **6**, their (*M*)- and (*P*)-conformers are enantiomers and thus equal in energy. However, when the C3 is monosubstituted, a stereogenic center is created and the two conformers will no longer be enantiomers. Sunjic first deduced the equatorial preference of the C3 methyl group in **11a** in solution.[45] Paizs studied **11a** and determined the two conformers differ in energy by 4.3 kcal/mol at B3LYP/6-31G(d).[39] According to these earlier studies, the (*S*)-enantiomer preferentially adopts (*M*)-helicity, since this conformation places the methyl group in the equatorial position.[46] With our success in asymmetric alkylation utilizing the *i*-Pr group as the N1 substituent, we focused our attention on the corresponding des-chloro *N*-*i*-Pr compound **12d** (Figure 5).

In agreement with Paizs's finding, two equilibrium geometries were found for the (*S*)-enantiomer, and the (*M*)-conformer (featuring an equatorial C3 methyl) is lower in energy by 5.2 kcal/mol. Selected structural

(42) Guner, V.; Khuong, K. S.; Leach, A. G.; Lee, P. S.; Bartberger, M. D.; Houk, K. N. *J. Phys. Chem. A* **2003**, *107*, 11445−11459.

(43) Based on standard bond angles for sp^2 and sp^3 atoms (120° and 109°, respectively). the sum of angles in the BZD ring (six sp^2 and one sp^3 atoms) should be approximately 829°.

(44) The sum of internal angles of a polygon is $(180n - 360)°$, where n is the number sides of the polygon.

(45) Sunjic, V.; Lisini, A.; Sega, A.; Kovac, T.; Kajfez, F.; Ruscic, B. *J. Heterocycl. Chem.* **1979**, *16*, 757−761.

(46) In these earlier studies (*M*)- and (*P*)-chirality were defined by the dihedral angle C2−C3−N4−C5. Although we assign chirality based on a different dihedral angle (C8−C7−N1−C9), our resultant axial chirality assignment is the same.

TABLE 4. Comparison of C3-Monosubstituted BZD 12d and Glycine-Derived BZD 6d Equilibrium Geometries[a]

compd	C3 methyl	∠N1−C2−C3−N4 (deg)	∠C2−C3−N4−C5 (deg)	sum of internal ∠[b] (deg)
(*M*)-**6d**	na	68.8	−72.9	832.6
(*M*)-(*S*)-**12d**	eq	69.6	−73.4	829.8
(*P*)-(*S*)-**12d**	ax	−59.0	64.1	843.9

[a] The structures are optimized at the B3LYP/6-31G(d) level. The axial chirality is defined by the C6−C7−N1−C2 dihedral angle. [b] Sum of the seven internal bond angles in the BZD's seven-membered ring.

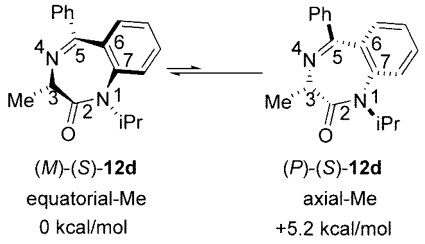

FIGURE 5. B3LYP/6-31G(d) energy difference between the (*P*)- and (*M*)-conformers of (*S*)-**12d**.

parameters of (*S*)-**12d** and the glycine-derived analogue **6d** are given in Table 4.

All of the structural parameters of equatorial methyl conformer (*M*)-(*S*)-**12d** are very similar to that of glycine analogue (*M*)-**6d**, suggesting that the equatorial Me group does not significantly alter the equilibrium geometry. However, the axial methyl conformer (*P*)-(*S*)-**12d** differs noticeably from (*M*)-**6d**, in the smaller dihedral angles N1−C2−C3−N4 and C2−C3−N4−C5. These differences are caused by the steric interaction between the axial Me group and the benzo ring, which in turn causes the seven-membered ring to adopt a flatter geometry, as reflected in the bigger sum of internal bond angles. Both the steric interaction and the ring flattening likely contribute to the destabilization of the axial (*P*)-(*S*)-conformer.

This equatorial preference has two implications in our "memory of chirality"[22] approach: (1) Because the (*S*)-enantiomer exists exclusively as the (*M*)-conformer (5.2 kcal/mol difference in energy corresponds to around 6500:1 equilibrium ratio at room temperature), the N1−C7 axis effectively "memorizes" the chirality of the stereogenic center at C3 in its equilibrium geometry. (2) The dihedral angle H3−C3−C2−O10 in the preferred equatorial-Me conformer is 133°, but is nearly eclipsed (6°) in the less favorable axial-Me conformer. Thus the lower energy equatorial conformer should also be most easily deprotonated.[47] Therefore, during the deprotonation to form its enolate, the preferred equatorial-Me conformer is the most reactive, and thus the chiral information preserved in its N1−C7 axis can be transferred to its enolate.

Ring-Inversion Process of C3 Monosubstituted BZD 12d. Paizs studied C3-monosubstituted BZD **11a** and reported only one transition structure for interconversion of the (*M*)- and (*P*)-conformational diastereomers.[39] In contrast, for the des-chloro *N*-*i*-Pr analogue (*S*)-**12d**, we located *two* ring-inversion transition structures. As in the case of **5b** and **6b**−**e**, the ring in the inversion transition structures is not completely flat and thus adopts an (*M*)- or (*P*)-conformation. Thus, the existence of two ring-inversion transition structures for (*S*)-**12d** is not unexpected. The presence of a chiral center at C3 of **12d** renders these two conformation diastereomeric, but otherwise the structures of (*M*)-(*S*)- and (*P*)-(*S*)-**12d*** closely mimic that of the glycine analogues (*M*)- and (*P*)-**6d*** (Figure 6). For (*S*)-**12d***, the (*M*)-conformer features an axial Me group, and the (*P*)-conformer features and equatorial Me group; the reverse would be true for (*R*)-**12d***.

Thus, two inversion pathways exist for each equilibrium geometry conformer. For the lower energy conformer (*M*)-(*S*)-**12d**, the barriers to inversion through the axial and equatorial transition structures are 21.5 and 22.5 kcal/mol, respectively. These calculated inversion barriers are very similar to that of **6d**, since in both cases no significant destabilization of equilibrium geometries is involved. Of course, for the higher energy conformer (*P*)-(S)-**12d**, the inversion barriers are lower (16.2 and 17.3 kcal/mol) due to destabilization of the equilibrium geometry.

^{1}H NMR Studies of a 3,3-Disubstituted "Quaternary" BZD 13d. Since C3-monosubstituted BZDs such as **12d** exhibit only one spectroscopically observable equatorial conformer, it has not yet been possible to experimentally determine the barrier to ring inversion. However, since unsymmetrically substituted quaternary BZDs typically display two slowly interconverting conformers, we chose to measure the rate of their interconversion. We synthesized (*R*)-**13d** according to the procedure we published recently[22] and measured its inversion barrier by coalescence temperature measurement (Figure 7). The two *i*-Pr Me groups coalesced at 380 K, which corresponds to an inversion barrier of 18.6 kcal/mol, significantly lower than that of the corresponding glycine analogue **6d** (21.3-21.7 kcal/mol). We propose the reason for this is again due to the steric interaction between the axial C3 substituent and the benzo ring. For **12d**, this steric interaction can be avoided by adopting the equatorial Me conformer, and this conformer is indeed the only observable one in the ^{1}H NMR spectrum. However, for C3 disubstituted **13d**, there is always an axial substituent no matter what conformation it adopts, and therefore, destabilization of the ground state is inevitable, causing a lower inversion barrier. The two conformers of **13d** are not equally populated, but at a 55:45 ratio, indicating an energy difference of 0.1 kcal/mol between the two conformers at room temperature. The major conformer is found to have an axial Me, equatorial Bn conformation by inspection of the ^{1}H NMR shifts of the two conformers, suggesting that the steric interaction between the benzo ring and the C3 benzyl group is slightly larger than that between the benzo ring and the C3 methyl group.

2D EXSY ^{1}H NMR Studies of 3,3-Disubstituted "Quaternary" BZD 13d. We studied the ring inversion

(47) Behnam, S. M.; Behnam, S. E.; Ando, K.; Green, N. S.; Houk, K. N. *J. Org. Chem.* **2000**, *65*, 8970−8978.

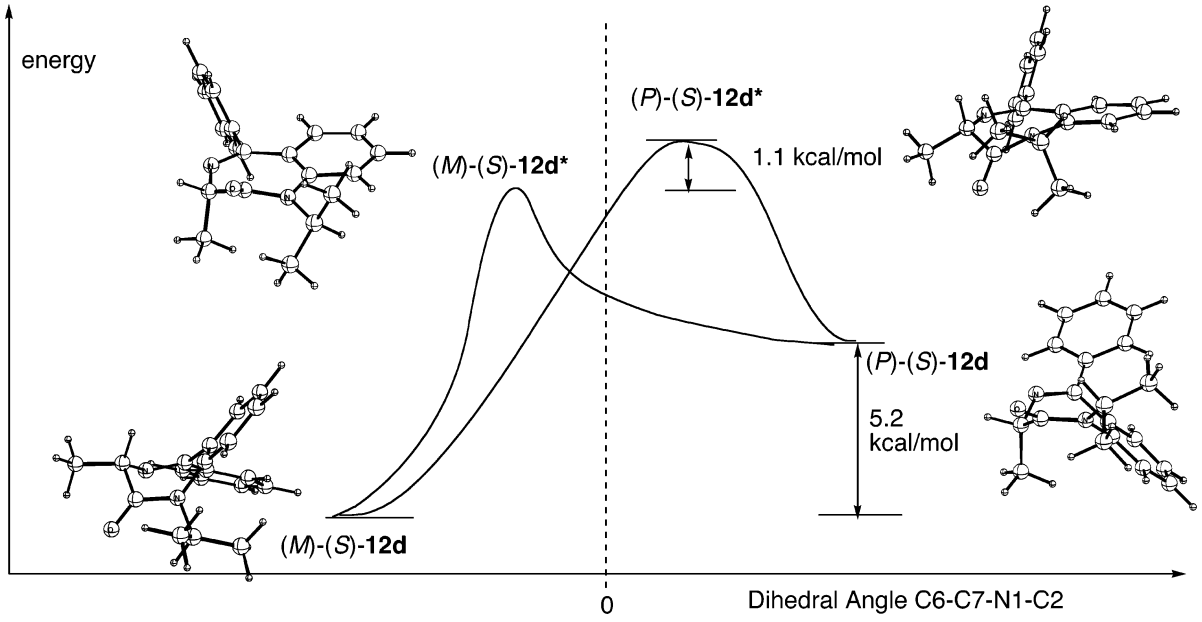

FIGURE 6. Ring-inversion process for (*S*)-**12d**. The equatorial Me equilibrium geometry (*M*)-(*S*)-**12d** is 5.2 kcal/mol lower in energy than its axial Me counterpart, (*P*)-(*S*)-**12d**. There are two ring-inversion transition structures: (*M*)-(*S*)-Me-**12d***, in which the C3 Me is axial, is 1.1 kcal/mol lower in energy than (*P*)-(*S*)-**12d***, in which the equatorial Me eclipses the C2 carbonyl. Note that the sign of the dihedral angle C6−C7−N1−C2 defines the helical chirality descriptor (*M* or *P*).

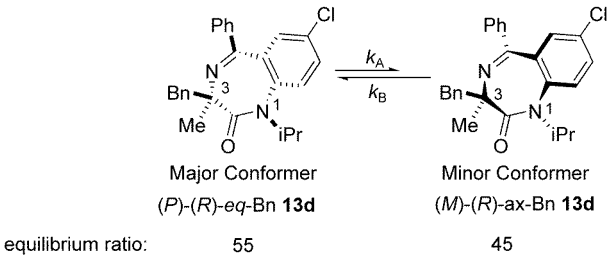

FIGURE 7. Major conformer *eq*-Bn-**13d** and minor conformer *ax*-Bn-**13d** observed by 2D-EXSY NMR.

process of **13d** by 2D-EXSY ^{1}H NMR, a technique which shares the same pulse sequence with 2D-NOESY.[48] The use of 2D-EXSY permits the determination of the forward inversion rate constant k_A, defined by the inversion from the major conformer (*eq*-Bn-**13d**) to the minor conformer (*ax*-Bn-**13d**), and the reverse inversion rate constant k_B, defined by the inversion from the minor conformer to the major conformer (Figure 7). Measurement of the exchange rates at different temperature T and the subsequent plots of $\ln(k_A/T)$ and $\ln(k_B/T)$ vs $1/T$ allows extrapolation of the activation parameters $\Delta H^{\ddagger}$ and $\Delta S^{\ddagger}$ for both the forward and reverse processes, which are shown in Figure 8.

The major conformer (∼55%) has the bulkier Bn group in the equatorial position; the minor conformer (∼45%) in contrast has an axial Bn group. The 2D-EXSY measurements show that the activations of enthalpy for the ring inversion of **13d** from the *eq*-Bn- and *ax*-Bn-conformers are 17.5 and 17.4 kcal/mol, respectively. Both of them show a small entropy of activation (less than −4 cal/mol/K). The free energy of activation for the major and minor conformers at 298 K are 18.6 and 18.5 kcal/mol, respectively, in close agreement with the value we obtained from the coalescence temperature study (cf. 18.9 and 18.8 kcal/mol at 380 K, the coalescence temperature). The 0.1 kcal/mol free energy difference we obtained from 2D-EXSY studies between the two conformers also corresponds well with the observed 0.55:0.45 composition in 1D ^{1}H NMR.

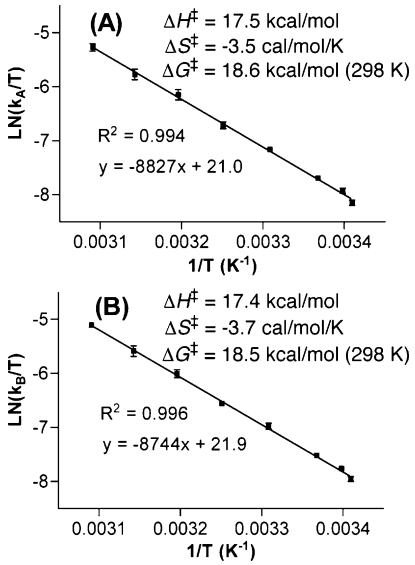

FIGURE 8. Plot of ln(*k*/T) versus 1/*T* for **13d** from 2D-EXSY measurements. From a total of 23 EXSY spectra measured at 293−324 K with varying t_m. There are two sets of exchanging protons in each spectrum; therefore there are a total of 46 data points. (A) Plot of exchange rate k_A from the major conformer (*eq*-Bn-**13d**). (B) Plot of exchange rate k_B from the minor conformer (*ax*-Bn-**13d**)

DFT Calculations of 3,3-Disubstituted "Quaternary" BZD 13d. The equilibrium geometry and ring-inversion transition structures of **13d** were determined at B3LYP/6-31G(d), and B3LYP/6-31+G(d) single-point energies were obtained using Tomasi's PCM model[40] with

(48) Perrin, C. L.; Dwyer, T. J. *Chem. Rev.* **1990**, *90*, 935−967.

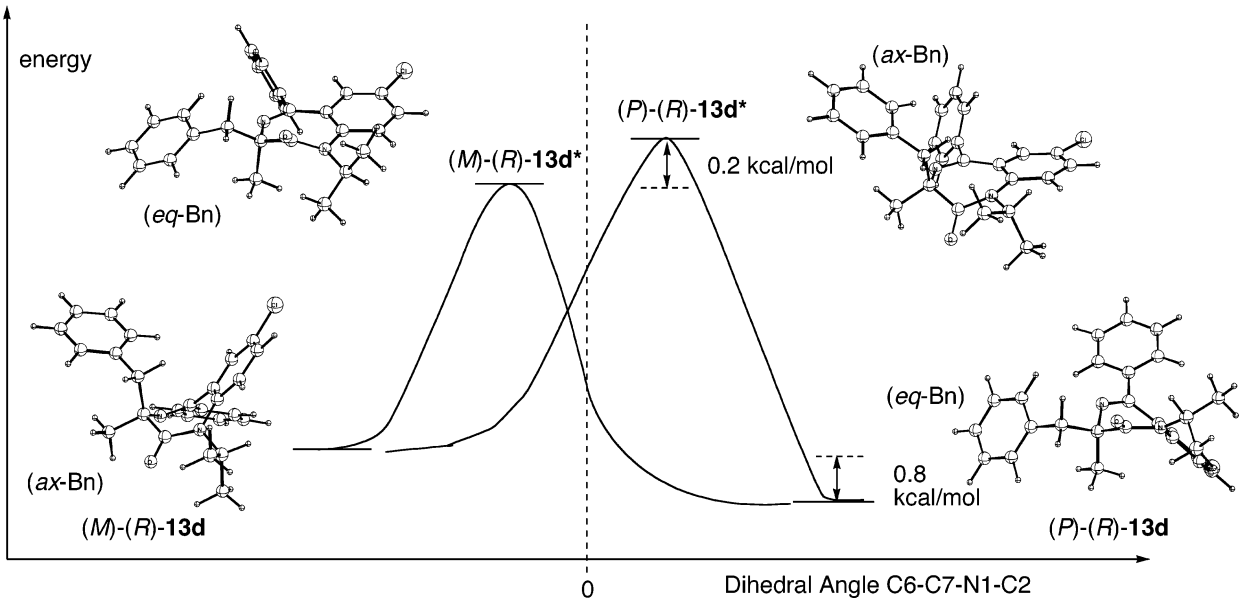

FIGURE 9. Ring-inversion process for (*R*)-**13d**. For equilibrium geometries, the equatorial Bn conformer (*P*)-(*R*)-**13d** is 0.8 kcal/mol lower in energy than the axial Bn counterpart, (*M*)-(*R*)-**13d**. Two nearly equienergetic ring- inversion transition structures (*M*)-(*R*)-**13d*** and (*P*)-(*R*)-**13d*** were located.

TABLE 5. DFT Calculations and Experimental Activation Parameters of Ring Inversion of 13d[a]

		B3LYP/6-31+G(d)//B3LYP/6-31G(d)			
EQ geom[b]	TS[c]	$\Delta G^{\ddagger}_{298}$ ($CHCl_3$)[d]	$\Delta H^{\ddagger}$ ($CHCl_3$)[e]	exptl $\Delta G^{\ddagger}_{298}$ ($CHCl_3$)[f]	exptl $\Delta H^{\ddagger}$ ($CHCl_3$)[g]
(*P*)-(*R*)-**13d** (eq-Bn)	(*M*)-(*R*)-**13d***	18.4	17.1	18.6	17.5
	(*P*)-(*R*)-**13d***	18.6	17.1		
(*M*)-(*R*)-**13d** (ax-Bn)	(*M*)-(*R*)-**13d***	17.6	16.2	18.5	17.5
	(*P*)-(*R*)-**13d***	17.8	16.2		

[a] The equilibrium geometries and transition structures are optimized at the B3LYP/6-31G(d) level with frequency calculations. Single-point energy calculations using Tomasi's PCM model in $CHCl_3$ were then performed at the B3LYP/6-31+G(d) level. The appropriate thermal correction to free energy or enthalpy, calculated from the vibrational data, is then applied to the single-point energy to yield the calculated activation parameters. [b] Two equilibrium geometries exist, the *eq*-Bn (*P*)-(*R*)-conformer is lower in energy, in agreement with NMR studies. [c] As for **5b**, **6b**−**e**, and **12d**, both (*M*)- and (*P*)-ring inversion transition structures were located. [d] The thermal correction to the Gibbs free energy is applied to yield the calculated Gibbs free energy of activation. [e] The thermal correction to enthalpy is applied to yield the calculated activation enthalpy. [f] Calculated at 298 K by extrapolating the 2D-EXSY experimental activation parameters. [g] Obtained from the 2D-EXSY studies.

$CHCl_3$ as the solvent. The thermal correction to the Gibbs free energy and enthalpy using vibrational data at 6-31G-(d) were applied to calculate the activation free energy and enthalpy. The results are summarized in Table 5.

In our calculations and NMR studies, the *eq*-Bn conformer (*P*)-(*R*)-**13d** is lower in energy than the *ax*-Bn conformer (*M*)-(*R*)-**13d**, as would be expected from the somewhat larger equatorial preference of the benzyl group relative to methyl. Our calculated free energy difference between the two conformers is 0.8 kcal/mol, slightly higher than the experimental value of 0.1 kcal/mol.

The scenario for ring inversion of **13d** is very similar to that of **12d**, both of which contain an asymmetrically substituted C3. Two diastereomeric ring-inversion transition structures were found; one contains an equatorial Bn and the other contains an axial Bn (Figure 9). In this case, the two ring-inversion transition structures (*M*)-(*R*)-**13d*** and (*P*)-(*R*)-**13d*** are nearly equienergetic, differing only by 0.2 kcal/mol. In general, our calculated activation parameters are within ∼1 kcal/mol of the experimentally determined $\Delta G^{\ddagger}$ and $\Delta H^{\ddagger}$ (Table 5). The calculated entropy of activation ranges from −4.4 to −5.5 cal/mol/K, which is quite close to the experimentally determined value of −3.5 to −3.7 cal/mol/K.

Conclusions

Using coalescence temperature measurements and 2D-EXSY ^{1}H NMR spectroscopy, we were able to determine the barriers and activation parameters of the ring inversion process of various BZDs. Using density functional theory, we were able to reproduce these results with good (within 1−2 kcal/mol) accuracy. We concluded that B3LYP/6-31G(d) is an adequate method for geometry optimization in the study of BZD systems and that single-point energy calculations incorporating diffuse functions, solvent effect, and thermal correction offer improved accuracy.

Calculated structural parameters of various BZDs provide valuable insights into their ring-inversion processes. Glycine-derived BZDs undergo ring inversion via a pair of enantiomeric ring-inversion transition structures, whereas tertiary or asymmetrically substituted quaternary BZDs possess two diastereomeric ring-inversion transition structures. Bulky N1 substituents (*i*-Pr and $CHPh_2$) distort the ring-inversion transition structure from planarity and disrupt amide resonance, thereby causing a higher inversion barrier. We also demonstrated how the equatorial preference of C3-monosubstituted BZDs provides the basis for the transmission of chiral

information from C3 to the N1−C7 axis during the memory of chirality deprotonation/alkylation. These studies have provided a foundation for the future studies of the BZD enolates.

Experimental Section

General Methods. THF was distilled from Na/benzophenone immediately before use. (*S*)-Boc-Ala was purchased from Advanced ChemTech and was used as received. Compounds **5a** and **5b** were prepared according to the literature method.[49] Compound **5c** was prepared from **5a** using a similar method, and the spectroscopic data matched those published.[50] Compound **5d** and **13d** were prepared according to our published procedure.[22] Compound (*S*)-**12d** was prepared from (*S*)-Boc-Ala using a modification of Shea's protocol.[30]

7-Chloro-1,3-dihydro-1-diphenylmethyl-5-phenyl-2*H*-1,4-benzodiazepin-2-one 5e. At 0 °C, to a stirred solution of **5a** (50.9 mg, 0.188 mmol, 1 equiv) and HMPA (196 μL, 1.13 mmol, 6.0 equiv) in dry THF (2.0 mL) was added NaH (11.3 mg, 0.282 mmol, 1.5 equiv, 60% suspension in mineral oil) in one portion. The resulting solution was stirred at 0 °C for 30 min before the dropwise addition of bromodiphenylmethane (155 mg, 0.564 mmol, 3 equiv). The reaction mixture was stirred overnight, quenched with 10 mL of saturated aqueous NH_4Cl solution, and extracted with CH_2Cl_2 (3 × 20 mL). The combined extracts were dried over anhydrous Na_2SO_4, filtered, and concentrated. The crude product was purified by flash column chromatography on silica gel to yield a white solid (78.7 mg, 0.180 mmol, 96% yield): mp 203.8−204.2 °C; ^{1}H NMR (DMSO-*d*) δ 4.06 (d, $^2J_{HH}$ = 10.8 Hz, 1H), 4.66 (d, $^2J_{HH}$ = 10.6 Hz, 1H), 6.90 (s, 1H), 6.97 (d, $^3J_{HH}$ = 6.7 Hz, 2H), 7.05 (d, $^4J_{HH}$ = 2.5 Hz, 1H), 7.18−7.44 (m, 11C), 7.45 (t, $^3J_{HH}$ = 7.5 Hz, 2H), 7.54 (t, $^3J_{HH}$ = 7.3 Hz, 1H), 8.32 (s, 1H); ^{13}C NMR ($CDCl_3$) δ 57.37, 64.70, 126.05, 127.45, 127.80, 127.95, 128.40, 128.44, 128.62, 129.29, 129.48, 130.03, 130.30, 130.33, 130.77, 132.67, 137.85, 138.00, 138.13, 139.86, 169.23, 169.38; HRMS (FAB) calcd for $C_{28}H_{22}N_2OCl$ $[M + H]^+$ 437.1421, found 437.1407 (−3.2 ppm, −1.4 mmu).

NMR Measurements. ^{1}H NMR spectra were recorded on either a JEOL Eclipse 500 or a Varian Inova 400 MHz NMR spectrometer; the corresponding ^{13}C NMR resonant frequencies were 125 and 100 MHz, respectively.

Dynamic ^{1}H NMR measurements were performed on a Varian Unity 400 MHz NMR spectrometer with a recently calibrated temperature control unit. The coalescence temperature was determined to the nearest 3 K, and therefore, the calculated inversion barrier carries an uncertainty of ± 0.2 kcal/mol.

2D EXSY ^{1}H NMR spectra were obtained on the Varian Inova 400 MHz NMR spectrometer with a recently calibrated temperature control unit, with ±0.1 K uncertainty in temperature. The relaxation times T_1 of all aliphatic protons of **13d** were measured at various temperature used, and the relaxation delay was set to be 4−5 times the longest T_1 at that temperature to ensure full relaxation between consecutive pulses. A total of 23 spectra were recorded at eight different temperatures, ranging from 293 to 324 K. Mixing time t_m of each measurement was set to be around the optimized value of $1/(T_1^{-1} + k_A + k_B)$ to maximize the extent of exchange.[48]

Computational Details

All DFT and MP2 calculations were done using either the Gaussian 98[51] or the Gaussian 03 program.[52] All equilibrium geometries and ring inversion transition structures are optimized at B3LYP/6-31G(d) level using the hybrid of Becke' three-parameter exchange functional (B3)[53] and Lee, Yang, and Parr's exchange-correlation functional.[54] Vibrational frequencies were calculated at the same level to verify the calculated structure as either minima (no imaginary frequency) or transition structure (single imaginary frequency). The vibrational vector of the transition structures' single imaginary frequency corresponds to the transformation from the transition structure toward either one of the equilibrium geometries. Zero-point vibrational energies and thermal corrections to enthalpies and Gibbs free energies,[55] calculated at 195 K, were calculated from corrected frequencies (correction factor: 0.9804).[56,57] Solvent effects were taken into account by single point energy calculation at B3LYP/6-31+G(d), using Tomasi's polarizable continuum model (PCM).[40] IRC calculations on the ring-inversion process of **6d** were performed starting from the ring-inversion transition structures (*M*)-**6d*** and (*P*)-**6d***. The Z-matrices of these starting geometries were constructed using internal coordinates, so that the six carbon and four hydrogen atoms on the benzo ring were held immobile, while all other geometric parameters were variables. Forward and reverse directions were calculated separately, using internal coordinates without mass weighing (nondefault setting) and the default step size of 0.1 amu$^{1/2}$−Bohr; 37 forward steps and 39 reverse steps were required to arrive at the equilibrium geometries on either side of the reaction coordinates.

Acknowledgment. We thank the National Science Foundation (CHE-0213525), the Jeffress Memorial Trust, and the Virgina Tech Department of Chemistry for financial support.

Supporting Information Available: NMR spectra of **5e**; atomic coordinates, energies of all the studied species, calculated geometries of all stationary points. This material is available free of charge via the Internet at http://pubs.acs.org.

JO048450N

(49) Sternbach, L. H.; Fryer, R. I.; Metlesics, W.; Reeder, E.; Sach, G.; Saucy, G.; Stempel, A. *J. Org. Chem.* **1962**, *27*, 3788−3796.

(50) Goumri-Magnet, S.; Guerret, O.; Gornitzka, H.; Cazaux, J. B.; Bigg, D.; Palacios, F.; Bertrand, G. *J. Org. Chem.* **1999**, *64*, 3741−3744.

(51) Frisch, M. J.; Trucks, G. W.; Schlegel, H. B.; Scuseria, G. E.; Robb, M. A.; Cheeseman, J. R.; Zakrzewski, V. G.; Montgomery, J. A., Jr.; Stratmann, R. E.; Burant, J. C.; Dapprich, S.; Millam, J. M.; Daniels, A. D.; Kudin, K. N.; Strain, M. C.; Farkas, O.; Tomasi, J.; Barone, V.; Cossi, M.; Cammi, R.; Mennucci, B.; Pomelli, C.; Adamo, C.; Clifford, S.; Ochterski, J.; Petersson, G. A.; Ayala, P. Y.; Cui, Q.; Morokuma, K.; Malick, D. K.; Rabuck, A. D.; Raghavachari, K.; Foresman, J. B.; Cioslowski, J.; Ortiz, J. V.; Stefanov, B. B.; Liu, G.; Liashenko, A.; Piskorz, P.; Komaromi, I.; Gomperts, R.; Martin, R. L.; Fox, D. J.; Keith, T.; Al-Laham, M. A.; Peng, C. Y.; Nanayakkara, A.; Gonzalez, C.; Challacombe, M.; Gill, P. M. W.; Johnson, B. G.; Chen, W.; Wong, M. W.; Andres, J. L.; Head-Gordon, M.; Replogle, E. S.; Pople, J. A. *Gaussian 98*, revision A.11.1; Gaussian, Inc.: Pittsburgh, PA, 1998.

(52) Frisch, M. J.; Trucks, G. W.; Schlegel, H. B.; Scuseria, G. E.; Robb, M. A.; Cheeseman, J. R.; Montgomery, J. A., Jr.; Vreven, T.; Kudin, K. N.; Burant, J. C.; Millam, J. M.; Iyengar, S. S.; Tomasi, J.; Barone, V.; Mennucci, B.; Cossi, M.; Scalmani, G.; Rega, N.; Petersson, G. A.; Nakatsuji, H.; Hada, M.; Ehara, M.; Toyota, K.; Fukuda, R.; Hasegawa, J.; Ishida, M.; Nakajima, T.; Honda, Y.; Kitao, O.; Nakai, H.; Klene, M.; Li, X.; Knox, J. E.; Hratchian, H. P.; Cross, J. B.; Adamo, C.; Jaramillo, J.; Gomperts, R.; Stratmann, R. E.; Yazyev, O.; Austin, A. J.; Cammi, R.; Pomelli, C.; Ochterski, J. W.; Ayala, P. Y.; Morokuma, K.; Voth, G. A.; Salvador, P.; Dannenberg, J. J.; Zakrzewski, V. G.; Dapprich, S.; Daniels, A. D.; Strain, M. C.; Farkas, O.; Malick, D. K.; Rabuck, A. D.; Raghavachari, K.; Foresman, J. B.; Ortiz, J. V.; Cui, Q.; Baboul, A. G.; Clifford, S.; Cioslowski, J.; Stefanov, B. B.; Liu, G.; Liashenko, A.; Piskorz, P.; Komaromi, I.; Martin, R. L.; Fox, D. J.; Keith, T.; Al-Laham, M. A.; Peng, C. Y.; Nanayakkara, A.; Challacombe, M.; Gill, P. M. W.; Johnson, B.; Chen, W.; Wong, M. W.; Gonzalez, C.; Pople, J. A. *Gaussian 03*, revision B.05; Gaussian, Inc.: Pittsburgh, PA, 2003.

(53) Becke, A. D. *J. Chem. Phys.* **1993**, *98*, 5648−5652.

(54) Lee, C.; Yang, W.; Parr, R. G. *Phys. Rev. B* **1988**, *37*, 785−789.

(55) McQuarrie, D. A.; Simon, J. D. *Molecular thermodynamics*; University Science Books: Sausalito, Calif., 1999; pp xiii, 656 pp.

(56) Scott, A. P.; Radom, L. *J. Phys. Chem.* **1996**, *100*, 16502−16513.

(57) Wong, M. W. *Chem. Phys. Lett.* **1996**, *256*, 391−399.